

*This paper evaluates potential accuracy characteristics of a small-sized goniometer based on nuclear magnetic resonance with an extended dynamic range. This required constructing a model of goniometer errors, estimating its accuracy based on this model, and formulating practical recommendations for the design of such a device based on the accuracy assessment.*

*To evaluate the accuracy of a nuclear goniometer, a theoretical model was built that makes it possible to determine the optimal operating parameters of the cell gas mixture, the ranges of their permissible changes, the sensitivity of the goniometer, and the dependence of its characteristics on external and internal factors. In particular, the dependence of output signal of the device on the parameters of gas mixture and optical pumping has been determined. For a goniometer with a cell volume of 8 cm<sup>3</sup>, the optimum temperature is 130 °C, and the optimum intensity of the pumping radiation is 5 mW.*

*The dependence of output signal on the measured angle of rotation was also established, as well as the noise and error dependence of the device on the permissible values of its parameters. Based on the model built, parameters of a goniometer with a cell volume of 8 cm<sup>3</sup> were determined; the maximum angular sensitivity of such a goniometer with complete suppression of technical noise is  $\delta\varphi_{sen}=1.0$  arcsec. The greatest contribution to the angle measurement error is from the instability of pumping power  $I_p$  ( $\Delta I_p/I_p=0.05$ ) – 85 %, magnetic field  $B_0$  ( $\Delta B_0/B_0=10^{-8}$ ) – 13 %, temperature  $T$  ( $\Delta T/T=0.1$ ) – 2 %.*

*The goniometer under consideration corresponds to the medium accuracy class,  $\delta\varphi_{tot}\geq 10$  arcsec. It could be used in optical manufacturing for operational control, calibration, and certification of optical products. To improve the angular accuracy of the goniometer, it is necessary to increase the stability of the laser pumping intensity*

*Keywords: goniometer, nuclear magnetic resonance, gas cell, optical pumping, Helmholtz coil, Larmor frequency*

# ASSESSING THE POTENTIAL ACCURACY OF A SMALL-SIZED GONIOMETER WITH EXTENDED DYNAMIC RANGE BASED ON NUCLEAR MAGNETIC RESONANCE

**Sergiy Ivanov**

PhD, Professor

Department of Robotics and Technical Systems

Educational and Research Institute of

Telecommunications

State University of Information and

Communication Technologies

Solomianska str., 7, Kyiv, Ukraine, 03110

E-mail: ivanov.sergiyvik@gmail.com

Received date 13.08.2024

Accepted date 15.10.2024

Published date 30.10.2024

**How to Cite:** Ivanov, S. (2024). Assessing the potential accuracy of a small-sized goniometer with extended dynamic range based on nuclear magnetic resonance. *Eastern-European Journal of Enterprise Technologies*, 5 (5 (131)), 13–25. <https://doi.org/10.15587/1729-4061.2024.313878>

## 1. Introduction

There are a number of tasks that require measuring the angular position of an object in real time, for example, in angle measuring systems of test benches, tracking antenna arrays, optical telescopes, etc. Dynamic goniometers are used to measure such parameters.

In optical production, an urgent task is the operational control and certification of the angles of optical products (for example, the zone of insensitivity to the speed of rotation (capture zone) of a laser gyroscope) and the index of glass refraction.

New opportunities in the field of angular measurements in the production of optical devices appear with the development of nuclear goniometers and the construction of measuring systems based on them. The nuclear goniometer is a sensor of angular movements in inertial space, the basis of which is the gyroscopic properties of the particles of gas mixture caused by the spin and orbital moments of atoms. In an inertial frame of reference, under the action of a magnetic field, the nuclear spin of noble gas (Xe) atoms precesses around a selected axis. With a stationary goniometer, the frequency of spin precession is determined by the magnitude of the magnetic field. In the case of angular movement of the sensor around the direction of the magnetic field (axis of sensitivity of the goniometer), the change in the precession frequency is registered by the shift in the Larmor frequency of the nuclear spins of the noble

gas. The potential capabilities of the nuclear goniometer are determined by fluctuations in the precession frequency. Measurement of the shift in the noble gas precession frequency is the basis of the operation of the nuclear goniometer.

Studying a new type of dynamic goniometer based on nuclear magnetic resonance is a relevant task when devising new state-of-the-art technologies in optical production.

## 2. Literature review and problem statement

The basis of modern dynamic goniometry are devices based on the Sagnac effect. Classical dynamic goniometers employ laser dynamic goniometry, which uses the properties of ring lasers. The principle of operation of the laser goniometer, as well as methods for increasing its measurement accuracy, are given in [1]. A drawback of the study is that the authors did not perform an analysis of device errors.

The use of a laser interferometer for angle measurement is also described in [2], while the goniometer was designed as a device capable of measuring the angle with an error of the order of 10 nrad. The disadvantage of such a device is its considerable dimensions – the length of one side of the square contour is 50 cm. In addition, in [2], the results of tests of the device are not given, which would confirm the declared accuracy, as well as the analysis of device errors.

In study [3], focusing on the calibration of a goniometer based on a laser interferometer, the stability of the scale factor of the device and its dependence on temperature, repeatability, and stability of the zero shift were experimentally investigated. The accuracy of the device is  $\pm 0.5''$ . Since the paper considers methods for calibrating the goniometer, it does not contain a theoretical analysis of the nature of the errors of the laser dynamic goniometer.

The authors of [4] designed a precise intelligent goniometric system based on a ring laser, a CMOS matrix, and an artificial neural network. Since the work focuses on the principles of construction of this system and the general algorithm of its operation, the authors of [4] also do not analyze the nature of errors of the laser dynamic goniometer.

Study [5] proposed a method for increasing the accuracy of the laser goniometer measurement, which makes it possible to reduce the influence of the zero drift and the errors of installing the interferometer on the rotary table, and the analysis of these errors is given. The measurement error of the device is  $\pm 0.4''$ . The shortcoming of the study is the lack of analysis of other errors, in particular those caused by the capture zone of the laser goniometer.

The nature of disturbances in the output signal of a laser goniometer is considered in many publications as it is of interest during practical application in various fields of technology. According to the results of the research analysis, the main contribution to the error of the laser goniometer is from technical fluctuations caused by the instability of the detuning of the radiation frequency with respect to the central frequency of the atomic transition. Normal fluctuations caused by the quantum nature of radiation determine the potential accuracy of a laser goniometer. The main disadvantage of the goniometer based on the laser interferometer is also the presence of a capture zone, which causes its insensitivity at low speeds of table rotation.

A dynamic goniometer with a fiber-optic circuit, the work of which is also based on the Sagnac effect, is discussed in papers [6, 7]. The authors of [6] considered a way to increase the accuracy of the goniometer by eliminating angular misalignment and obtained an angle measurement accuracy of  $2''$ . Due to the limited scope of the study, the authors neglected one of the main causes of errors in fiber-optic goniometers – temperature instability due to the Shupe effect, citing papers that consider the similar error of fiber-optic gyroscopes. Paper [7] tackles the principle of operation and the analysis of the results of fiber-optic goniometer. The mathematical model of measurement result errors obtained by the authors of [7] is suitable for practical application and showed a good agreement with the experiment at a confidence probability of 95%. The authors did not conduct a theoretical analysis of the goniometer errors, focusing on the construction of a model of errors in the results. In [8], the author considered the emergence of a parasitic signal at the output of a fiber-optic gyroscope during a change in external temperature, as well as due to self-heating of the device and the action of mechanical loads. The author of this paper provided recommendations and requirements for the design of the sensitive elements of fiber optic gyroscopes to reduce the influence of the Shupp effect. However, even using these recommendations does not make it possible to completely get rid of this effect.

One can see from the above data that the main disadvantage of dynamic goniometers based on the Sagnac effect is the presence of a capture zone (devices based on ring lasers) and temperature stability (fiber-optic devices).

The task of designing a dynamic goniometer, free from the mentioned shortcomings, has not yet been solved. The reason for this is the fundamental impossibility of getting rid of errors without changing the principle of action of the sensitive element of the goniometer. An option to overcome these reasons can be the use of a goniometer based on nuclear magnetic resonance, the principle of operation of which is based on spin-exchange pumping. This type of goniometer is free from the drawbacks of Sagnac-based goniometers and could potentially be highly accurate at small dimensions. The advantages of the nuclear goniometer are insensitivity to overloads, long service life, digital output. All this gives reason to claim that it is expedient to conduct a study aimed at analyzing the accuracy of such a goniometer.

---

### 3. The aim and objectives of the study

---

The purpose of this study is to evaluate the potential accuracy characteristics of a goniometer with an extended dynamic range based on nuclear magnetic resonance and to devise practical recommendations for designing such a device based on it. This will make it possible to measure angles at low rotation speeds when manufacturing objects of complex shape, for example, large mirrors. It will also make it possible to organize operational control and certification of the angles of optical products and the index of glass refraction in optical production.

To achieve the defined goal, the following tasks were set:

- to determine the dependence of output signal on the parameters of gas mixture, optical pumping;
- to determine the dependence of output signal on the measured angle of rotation, analyze the noise and the dependence of device error on the permissible values of its parameters.

---

### 4. The study materials and methods

---

The object of research is dynamic goniometers for measuring the angles formed by flat surfaces of various objects capable of reflecting light rays. The main hypothesis assumes that the use of a small-sized sensitive element based on nuclear magnetic resonance would make it possible to simplify the design, reduce the energy consumption of the goniometer, its dimensions, and ensure measurements at low speeds. Dynamic laser goniometers cannot perform measurements at low speeds of rotation of the object table due to the presence of a capture zone.

The methods of spectral and mathematical analysis, signal theory, the theory of random processes and its engineering applications, the theory of nuclear magnetic resonance, methods from the electromagnetic theory of light, and the Jones matrix method were used in the research process. Modeling was carried out in the MATLAB, Mathcad environment using authentic software.

---

### 5. Investigating the potential accuracy characteristics of nuclear goniometer

---

#### 5.1. Investigating the dependence of amplitude of the output signal of the nuclear goniometer on the parameters of gas mixture and optical pumping

Fig. 1 shows the scheme of a nuclear goniometer [9], the main elements of which are a radiation source, a gas cell, a photo recorder, and coil systems for generating magnetic fields.

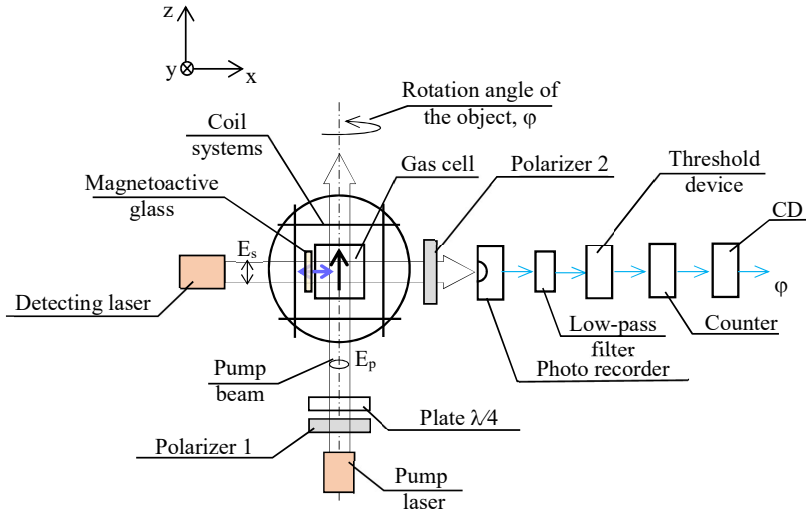


Fig. 1. Schematic showing the sensitive element of the nuclear goniometer

The cubic gas cell contains pairs of the isotope of the alkali metal rubidium  $^{87}\text{Rb}$  (gyromagnetic ratio  $\gamma_{\text{Rb}}=28 \text{ GHz/T}$ ), two isotopes of xenon noble gases  $^{129}\text{Xe}$  and  $^{131}\text{Xe}$  (gyromagnetic ratios  $\gamma_{129}=-11.9 \text{ MHz/T}$  and  $\gamma_{131}=3.52 \text{ MHz/T}$ , respectively) and buffer gas nitrogen  $\text{N}_2$ , placed between two non-magnetic heating plates inside the protective magnetic screen, which minimizes the influence of the Earth's magnetic field (induction of the external static magnetic field  $B_E=50 \mu\text{T}$ ). The temperature of the cell is kept constant, the operating point is selected in the range from 100 to 200 °C, taking into account ensuring the accuracy of the angle measurement. The cell is placed in a constant longitudinal magnetic field  $B_0$  greater than  $1 \mu\text{T}$  ( $1 \cdot 10^{-2} \text{ G}$ ), uniform throughout the volume, directed along the  $z$  axis, which determines the precession frequencies of the nuclear magnetization of the isotopes  $^{129}\text{Xe}$  and  $^{131}\text{Xe}$  and the resonance frequency of the electron paramagnetic resonance of the  $^{87}\text{Rb}$  atoms.

A transverse alternating magnetic field  $B_1 \sim (1 \text{ nT} = 10^{-9} \text{ T})$  is also superimposed on the cell, which is several orders of magnitude weaker than  $B_0$ . Field  $B_1$  contains two harmonic components with frequencies  $\omega'_{129}$  and  $\omega'_{131}$ , close to the natural precession frequencies,  $\omega_{129,131} = \gamma_{129,131} B_0$ , and excites nuclear magnetic resonance in isotopes  $^{129}\text{Xe}$  and  $^{131}\text{Xe}$ . The transverse alternating magnetic field  $B_1$  is created by the currents flowing in the windings of the Helmholtz coils. For certainty, in Fig. 1 the field  $B_1$  is directed along the  $x$ -axis. Under the action of the magnetic field  $B_1$ , the angular moments of the Rb atoms deviate from the  $z$  axis and perform a precessional movement around it. Atoms whose precession phases are coherent create in the medium a component of polarization of the medium transverse to the  $z$  axis by angular momentum. Optical radiation  $E_s$  with linear polarization propagating perpendicular to the  $z$  axis is used for its detection.

To orient the magnetic moments of  $^{87}\text{Rb}$  atoms, optical pumping is used at the resonance frequency of the  $D_1$   $^{87}\text{Rb}$   $5S_{1/2}^2 \rightarrow 5P_{1/2}^2$  ( $\lambda_{D1}=795 \text{ nm}$ ). A pump beam  $E_p$  with circular polarization passes through the cell along the  $z$ -axis parallel to the constant magnetic field  $B_0$ . In this process, the photon's angular momentum is transferred to the  $^{87}\text{Rb}$  atom, changing the state of its magnetic moment. As a result of the absorption of light in the cell, the atomic magnetic moments of  $^{87}\text{Rb}$  are partially oriented in the direction of the permanent magnetic field  $B_0$ . Xenon atoms do not interact with

light, since all their electron shells are filled, therefore, the alkali metal  $^{87}\text{Rb}$  is used to pump and read the polarization of Xe. The laser radiation power at the input of the cell  $I_p$  must be sufficient for the formation of spin polarization of Rb atoms, and the width of the laser emission line  $\Delta\nu_p$  is consistent with the width of the absorption line of Rb  $\Delta\nu_{\text{Rb}}$ . The lifetime of Rb atoms is limited by collisions and is inversely proportional to the pressure of the gas mixture. The line width of the Lorentzian contour  $\Delta\nu_{\text{Rb}}$  is proportional to the gas concentration, or equivalent to its pressure, and is determined by the natural width of the spectral line  $\Delta\nu_{\text{nat}}$ . The width of the spectral line is related to the probability of spontaneous emission and to the repulsive broadening caused by the interaction of Rb atoms with X atoms of the gas mixture:

$$\Delta\nu_{\text{Rb}} = \Delta\nu_{\text{nat}} + \sum k_x p_x, \quad (1)$$

where  $\Delta\nu_{\text{nat}}=5.7 \text{ MHz}$  is the natural width of the  $^{87}\text{Rb}$  line,  $k_x$  is the coefficient depending on gas X,  $p_x$  is the partial pressure of gas X.

Surface-emitting lasers with a vertical cavity (VCSEL) with a wavelength  $\lambda=795 \text{ nm}$ , power  $I \sim (0.5 \dots 10) \text{ mW}$ , radiation line width  $\Delta\nu_p \sim (0.5 \dots 1.0) \text{ GHz}$  can be used as a source of radiation in subsystems of optical pumping and detection of a nuclear goniometer; polarizer 1 and plate  $\lambda/4$  are used to obtain circularly polarized radiation.

The broadening of the Rb absorption line due to pressure (1) can be estimated using the following empirical formula [10]:

$$\Delta\nu_{\text{Rb}} \cong \frac{18.9n_{\text{Xe}} + 17.8n_{\text{N}_2}}{2.69 \cdot 10^{19}}, \quad (2)$$

where  $n_X$  is the concentration of gas medium components  $^{129}\text{Xe}$  and  $\text{N}_2$  in  $\text{cm}^{-3}$ .

Inside the cell there is  $\sim 2 \text{ g}$  of  $^{87}\text{Rb}$ , its melting point is 39 °C. At room temperature, Rb is in a solid state, the vapor pressure is  $\sim 10^{-7} \text{ Pa}$ . As the temperature rises, the concentration of Rb vapors increases almost exponentially, the liquid and gaseous phases are in constant dynamic equilibrium with respect to each other. The temperature dependence of the concentration of saturated Rb vapors is determined according to [11]:

$$n_{\text{Rb}}(T) = \frac{10^{\left(\frac{10.55 \cdot 4.132}{T}\right)}}{1.38 \cdot 10^{-16} \cdot T}, \text{ cm}^{-3}, \quad (3)$$

where  $n_{\text{Rb}}$  is the concentration of Rb in  $\text{cm}^{-3}$ ,  $T$  is the temperature of the gas cell in K.

In the gas cell, the Rb concentration can take on values from  $n_{\text{Rb}}=55.8 \cdot 10^{12} \text{ cm}^{-3}$  at  $T=100 \text{ °C}$  to  $n_{\text{Rb}}=10^{15} \text{ cm}^{-3}$  at  $T=200 \text{ °C}$  and can be controlled by the temperature used to optimize optical pumping. When filling the cell with a gas mixture under normal conditions (NC), the pressure of each  $^{129}\text{Xe}$  and  $^{131}\text{Xe}$  isotope is  $\sim (1 \dots 30) \text{ Torr}$ . To reduce the free flight time and relaxation rate on the cell walls, the concentration of  $^{129}\text{Xe}$  and  $^{131}\text{Xe}$  isotopes should be

(4...6) orders of magnitude greater than the concentration of Rb atoms. In order to increase the efficiency of the <sup>87</sup>Rb–Xe spin-exchange interaction, nitrogen N<sub>2</sub> buffer gas, which does not interact with laser radiation, is used. The pressure of N<sub>2</sub>~(20...80) Torr under NC, the concentration of n<sub>N2</sub>~(10<sup>17</sup>...10<sup>20</sup>) cm<sup>-3</sup> also exceeds the concentration of active Rb atoms by (4...6) orders of magnitude, which is due to the need to quench reradiation during absorption of the pump laser field.

The temperature dependences of the gas components Xe and N<sub>2</sub> are described by the equation of state of an ideal gas

$$p_i = n_i k_B T, \tag{4}$$

where n<sub>i</sub> is the concentration of the component of the i-th gas mixture, k<sub>B</sub> is the Boltzmann constant.

The temperature effect on the cell changes the pressure and concentration of Rb vapors, while the components of the gas mixture Xe and N<sub>2</sub> change only the pressure.

Under the influence of a static magnetic field B<sub>0</sub> and optical pumping E<sub>pp</sub>, an ensemble of Rb atoms is created in the gas cell with magnetic moments μ<sub>Rb</sub> oriented in one direction, which precess with the Larmor frequency ω<sub>Rb</sub> around the z axis; as a result, macroscopic magnetization M<sub>Rb</sub> appears, as shown in Fig. 2. Magnetization corresponds to the vector sum of individual magnetic moments of atoms in a unit volume of a gas cell  $\bar{M} = n \langle \mu \rangle$ . The magnetic moment of an atom <sup>j</sup>Xe is parallel to the nuclear spin I<sub>jXe</sub> and is related to it by the ratio μ<sub>jXe</sub>=g<sub>jXe</sub>I<sub>jXe</sub>μ<sub>N</sub>, where g<sub>jXe</sub> are g-factors of Xe isotopes, (for <sup>129</sup>Xe g<sub>129Xe</sub>=1.556, for <sup>131</sup>Xe g<sub>131Xe</sub>=0.461) I<sub>jXe</sub> – nuclear moments of Xe isotopes (for <sup>129</sup>Xe I<sub>129Xe</sub>=1/2, for <sup>131</sup>Xe I<sub>131Xe</sub>=3/2), μ<sub>N</sub> =  $\frac{e}{2m_p} = 5.050783 \cdot 10^{-27}$  J/Tl – nuclear magneton.

Since the gyromagnetic ratios γ<sub>129</sub> and γ<sub>131</sub> have different signs, the Larmor precession of Xe isotopes occurs in opposite directions. After a sufficient time, Xe atoms acquire nuclear magnetization  $\bar{M}_{129,131}$  and begin to precess around the applied magnetic field B<sub>0</sub> with their Larmor frequencies ω<sub>129,131</sub>. In the absence of the B<sub>1</sub> field, due to the stochastic phase precession of individual magnetic moments  $\bar{M}_{129,131}$  in the xy plane, the average transverse magnetization of Xe is zero. In the case of superposition of a transverse alternating magnetic field B<sub>1</sub> at frequencies close to the nuclear magnetic resonance of two isotopes <sup>129</sup>Xe and <sup>131</sup>Xe perpendicular to B<sub>0</sub>, the frequency of the Larmor precession of the nuclear magnetic moments of Xe isotopes under the action of an external force synchronize with the phase B<sub>1</sub> and the spins of Xe nuclei precess around the field B<sub>0</sub> with the same phase. In the xy plane, the rotating component of the total vector of macroscopic nuclear magnetization appears, rotating  $\bar{M}_{xyXe}$  and, therefore, along the x and y axes – the variable components M<sub>xXe</sub> and M<sub>yXe</sub>, as shown in Fig. 3.

The equation for the precession of the nuclear magnetization of <sup>j</sup>Xe isotopes in a constant magnetic field B<sub>0</sub> takes the form:

$$\begin{aligned} M_j(t) &= M_{xyj} \cos(\omega_j t + \varphi_j) \bar{e}_x + \\ &+ M_{xyj} \sin(\omega_j t + \varphi_j) \bar{e}_y + M_{zj} \bar{e}_z, \end{aligned} \tag{5}$$

where j=129, 131, M<sub>j</sub>(t) is the magnetization of a unit volume created by isotopes <sup>129</sup>Xe and <sup>131</sup>Xe, M<sub>xyj</sub> are the transverse components of the nuclear magnetization of the isotopes,

M<sub>zj</sub> are the longitudinal components of the nuclear magnetization, φ<sub>j</sub> are the precession phases of magnetization,  $\bar{M}_j$  in the xy plane, e<sub>q</sub> – unit vector along the q-th axis.

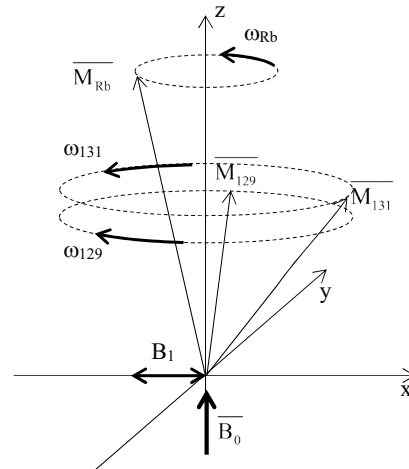


Fig. 2. Macroscopic magnetization vectors of the goniometer:  $\bar{M}_{131}$  – nuclear magnetization vectors of <sup>129</sup>Xe and <sup>131</sup>Xe, respectively,  $\bar{M}_{Rb}$  – Rb<sup>87</sup> spin magnetization vector

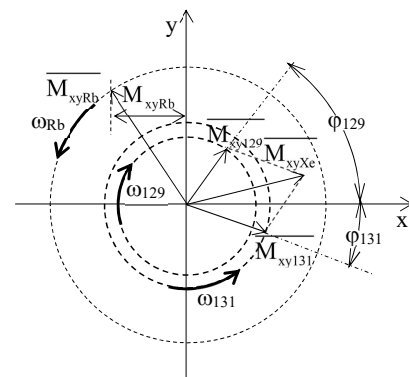


Fig. 3. Transverse projections of macroscopic magnetization vectors:  $\bar{M}_{xy129}, \bar{M}_{xy131}$  – transverse components of nuclear magnetization of Xe isotopes,  $\bar{M}_{xyXe}$  – transverse component of total vector  $\bar{M}_{xy129} + \bar{M}_{xy131}$ ,  $\bar{M}_{xyRb}$  – transverse component of electronic polarization Rb

From the geometric constructions in Fig. 3, it follows that the time dependences of the amplitude of the transverse component of the total vector M<sub>xyXe</sub> and the rotation angle φ<sub>xy</sub> of this vector relative to the x axis take the form:

$$M_{xyXe}(t) = \sqrt{M_{xy129}^2 + M_{xy131}^2 + 2M_{xy129}M_{xy131} \cos((\omega_{129} - \omega_{131})t + \varphi_{129} - \varphi_{131})}; \tag{6}$$

$$\begin{aligned} \varphi_{xy}(t) &= \\ &= \arctg \left[ \frac{M_{xy129} \sin(\omega_{129}t + \varphi_{129}) + M_{xy131} \sin(\omega_{131}t + \varphi_{131})}{M_{xy129} \cos(\omega_{129}t + \varphi_{129}) + M_{xy131} \cos(\omega_{131}t + \varphi_{131})} \right]. \end{aligned} \tag{7}$$

The nuclei of the precessing Xe isotopes create an additional magnetic field B<sub>jXe</sub>, which is sensed by the Rb atoms. In the assumption that the magnetization of Xe is uniform throughout the cell, the magnetic field

$$B_{jXe} = k_0 \frac{2}{3} \mu_0 (g_{jXe} I_{jXe} \mu_N) n_{jXe} M_{jXe} = k_B^{jXe} n_{jXe} M_{jXe}, \quad (8)$$

where  $k_0 \sim (400-760)$  is the Rb – Xe spin exchange amplification factor,  $\mu_0 = 4\pi \cdot 10^{-7}$  Hn/m is the magnetic constant,  $k_B^{jXe} = k_0 \frac{2}{3} \mu_0 (g_{jXe} I_{jXe} \mu_N)$ . The induction of the magnetic field  $\vec{B}(t)$  in which the  $^{87}\text{Rb}$  atoms are located is given in the form of the sum of three components: the longitudinal magnetic field  $B_0$ , the variable transverse magnetic field  $B_1$  and the nuclear magnetization field  $B_{jXe}$ , which depends on the state of the gaseous medium:

$$\vec{B}(t) = \overline{B_0(t)} + \overline{B_1(t)} + \overline{B_{jXe}(t)}. \quad (9)$$

The detecting laser linear radiation  $E_s$  interacts with the magnetic field of electrons Rb and, according to the Faraday effect, its plane of polarization turns to an angle  $\varepsilon$  proportional to  $M_{x\text{Rb}}$  – the projection of  $M_{\text{Rb}}$  on the  $x$  axis. Before entering the cell, the polarization plane  $E_s$  is perpendicular to the  $xy$  plane, after its passage the angle of inclination of the polarization plane changes relative to the  $z$  axis by the amount  $\varepsilon(t) \sim M_{x\text{Rb}}$ . The magnetizations of Rb and Xe are connected by a linear relationship, therefore, the magnitude of the angle  $\varepsilon$  determines the magnetization of Xe and the precession frequency  $\omega_j$  of the  $^j\text{Xe}$  isotopes:

$$\begin{aligned} \xi(t, \omega_r) &\sim M_{xy129} \cos[\varphi(t, \omega_r)] = \\ &= M_{xy129} \cos(\omega_{129}t + \varphi_{129}) + M_{xy131} \cos(\omega_{131}t + \varphi_{131}). \end{aligned} \quad (10)$$

The detecting beam  $E_s$  enters the photo recorder after passing through the magneto-active glass, cell, polarizer 2, which is installed behind the cell along the path of the beam in the extinguishing position at  $B_1=0$  and  $\omega_r=0$ . Magnetoactive glass, the cell are in the magnetic field  $B_1$  of the Helmholtz coils. The photo current of the photo recorder  $i_\varphi$  is proportional to the radiation power  $I$  falling on its photosensitive area. The electrical signal  $i_\varphi$  is a periodic oscillation with a modulated carrier, the amplitude of which varies from zero to  $A_m$  – the amplitude of the modulating signal. The isolation of the modulating oscillation is carried out by a low-pass filter, the cut-off frequency of which is greater than the maximum value of  $\omega_r$ . At the zero points of this signal, pulses are generated by the threshold device, which enter the counter  $i$ , then are processed by the computing device (CD) and the angle of rotation of the object  $\phi$  is determined.

In the inertial coordinate system, the vector  $\vec{M}_j$  precesses around the magnetic field  $\vec{B}_0$  induction vector with frequency  $\omega_j = \gamma_j B_0$  (Fig. 2), which is the result of statistical averaging of independent informative one-time measurements of the precession frequency of each  $^j\text{Xe}$  atom. The number of independent informative one-time measurements of the precession frequency  $N_v$  per unit of time is considered to be the signal  $S$ , and noise is the root mean square deviation  $\sigma_v$  of the number of all registered independent one-time measurements. Measurements are recorded per unit of time, from the average value of  $\langle N_v \rangle$ .  $\langle N_v \rangle$  is the average number of measurements during time  $t$ ,  $\langle N_v^2 \rangle$  is the average value of the square of  $\langle N_v \rangle$ ,  $\langle N_v \rangle^2$  is the square of the average value of  $\langle N_v \rangle$ . The average number of measurements for time  $t$  is  $N_{(v)} = S \cdot t$ , i.e.,  $S = \frac{\langle N_v \rangle}{t}$  measurements are recorded for a unit time interval, the average frequency of precession is  $\langle \omega \rangle = \frac{1}{S} \sum_{i=1}^S \omega_i$ .

Let the probability distribution density of a random process be determined by the normal law:

$$p(x) = \frac{1}{\sqrt{2\pi} \cdot \sigma_x} \exp\left[-\frac{(x - \langle x \rangle)^2}{2\sigma_x^2}\right], \quad (11)$$

where  $\langle x \rangle$  is the constant component of the random process,  $\sigma_x^2$  is the average power of the fluctuating component of the random process  $x(t)$ ,  $\sigma_x$  is the root mean square deviation.

The maximum time interval during which a single measurement of the precession frequency of an electron or nuclear magnetic moment can be carried out is equal to the relaxation time of this moment  $T_2$ , which is inversely proportional to the relaxation rate  $R_{tot}$  ( $T_2 = \frac{1}{R_{tot}}$ ). The transverse relaxation time of Rb atoms  $T_2^{\text{Rb}}$  is inversely proportional to the relaxation rate  $R_{tot} = R_{op} + R_{\text{Rb}}$  ( $T_2^{\text{Rb}} = \frac{1}{R_{op} + R_{\text{Rb}}} = \frac{1}{\pi \Delta\nu_{\text{Rb}}}$ ),

where  $R_{op}$  is the speed of the optical pumping,  $R_{\text{Rb}}$  is the rate of spin relaxation of Rb atoms ( $5S_{1/2}^2$  state decay rate), which is the sum of possible collisional interactions. The maximization of the pumping speed  $R_{op}$  is achieved by maintaining the balance of the vapor concentration Rb, the intensity of the light beam  $I_p$ , the width of the emission line  $\Delta\nu_p$ , the width of the absorption line  $\Delta\nu_{\text{Rb}}$ . During the calculation, it is assumed that the cell is completely illuminated by a collimated uniform light beam. The relaxation times of Rb and Xe are determined by Rb $\leftrightarrow$ Xe collisions, so the transverse relaxation times of Xe isotopes depend on their concentrations:

$$T_2^{jXe} = \frac{n_{jXe}}{n_{\text{Rb}} R_{\text{Rb}}}. \quad (12)$$

The polarization vector is defined by the relation:

$$\overline{P(t)} = \frac{\overline{M(t)}}{M_{\text{max}}}, \quad (13)$$

where  $M_{\text{max}}$  is the maximum possible magnetization at which all magnetic moments of atoms are parallel to  $B_0$ .

The spin polarization of a unit volume Rb along the  $z$  axis from the entrance window of the cell takes the form [12]:

$$\langle P_z \rangle = \frac{R_{op}}{R_{op} + R_{\text{Rb}}}. \quad (14)$$

When the cell is illuminated by monochromatic light  $E_p$ , the optical pumping speed  $R_{op}$  is proportional to the pumping intensity,  $R_{op} = \alpha \cdot I_p(z)$ , where  $\alpha$  is a coefficient that depends on the absorption cross section,  $I_p(z)$  is the intensity of the pumping beam at a distance  $z$  from the entrance window of the cell. Then the polarization Rb is determined from the following formula:

$$P_{\text{Rb}}(z) = \frac{I_p(z)}{I_p(z) + \frac{R_{\text{Rb}}}{\alpha}}. \quad (15)$$

Spin-polarized  $^{87}\text{Rb}$  atoms collide with Xe atoms, during which spin polarization exchange occurs. In the spin-exchange process, the polarization of Rb atoms is transferred

to <sup>129</sup>Xe and <sup>131</sup>Xe isotopes. In the first approximation, this dependence can be considered linear:

$$\langle P_{Xe} \rangle = \alpha \langle P_{Rb} \rangle = \frac{\alpha \cdot R_{op}}{R_{op} + R_{Rb}}, \quad (16)$$

where  $\alpha$  is the polarization transfer coefficient  $\langle P_{Rb} \rangle \leftrightarrow \langle P_{Xe} \rangle$  which depends on the parameters of the gas mixture.

The polarizations of Rb and Xe depend on temperature, pumping power, N<sub>2</sub> pressure, and Xe pressure.

The maximum output signal (corresponding to  $P=1$ ) is determined by the total number of  $N_{at}$  atoms and their relaxation time:

$$S_{max} = \frac{N_v}{t} = \frac{N_{at}}{T_2}, \quad (17)$$

where  $N_{at}$  is the number of atoms interacting with the field.

The real signal of the goniometer is created only by polarized atoms and is determined from the following expression:

$$S = P \frac{N_{at}}{T_2}, \quad (18)$$

where  $P$  is the polarization of the medium, which is equal to the relative fraction of atoms that are in non-equilibrium states,  $N_{at} = n_{at}V$  – the number of atoms (nuclei) in the volume of the cell  $V$ ,  $T_2$  – the time of a single measurement (transverse relaxation time).

The maximum signal on Rb atoms (at  $P=1$ ) takes the form:

$$S_{max}^{Rb} = \frac{n_{Rb}V}{T_2^{Rb}} = (R_{op} + R_{Rb})n_{Rb}V. \quad (19)$$

Amplitudes of signals from Xe isotopes (taking into account (12), (16)) are equal to:

$$S_{jXe} = P_{Xe} \frac{n_{jXe}V}{T_2^{jXe}} = \alpha \frac{R_{op}R_{Rb}}{R_{op} + R_{Rb}} n_{Rb}V. \quad (20)$$

The maximum amplitude of the transverse polarization of Rb atoms at the frequency  $\omega_{Xe} = \gamma_{Xe}B_0$  is proportional to the  $P_{Rb}$  polarization:

$$P_x^{Rb} \cong k_{tr} P_{Rb} B_{jXe}, \quad (21)$$

where  $k_{tr} \sim \gamma_{Rb} T_2^{Rb}$  is the conversion factor of the magnetic field created by Xe isotopes into the transverse component of Rb polarization.

The amplitude of the output signal of the goniometer is determined from the expression:

$$S_{out} = k_1 P_x^{Rb} S_{max}^{Rb}, \quad (22)$$

where  $k_1$  is the proportionality factor.

The amplitude  $S_{out}$  is proportional to the spin component  $P_x$  along the detector beam, the number of polarized atoms Rb. Fig. 4 shows the plot of  $S_{out} = F(T, I_p)$  as a surface represented by a function of temperature in the cell and the laser pump power.

As the temperature  $T$  and the pumping power  $I_p$  increase, the output signals  $S_{out}$  on <sup>j</sup>Xe isotopes increase. The  $S_{out}$  signal on <sup>131</sup>Xe atoms is larger than on <sup>129</sup>Xe.

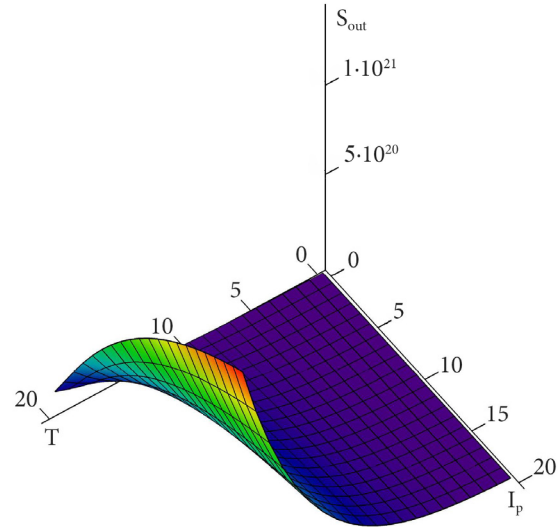


Fig. 4. Output signal of the goniometer, represented in the form of a surface from two variables – cell temperature  $T$  and laser pumping power  $I_p$ ,  $S_{out} = F(I_p, T)$

## 5. 2. Investigating the angular error of nuclear goniometer from its natural noise and fluctuations in external parameters

### 5. 2. 1. Method for measuring the angle of rotation of the object

The angular displacement of the object is determined by the measurement time  $t$  and the precession frequency  $\omega_r$ . To highlight the slow precession of the nuclear magnetization  $\omega_r$  in the scheme of the sensitive element of the goniometer (Fig. 1), a magneto-active glass is installed in front of the cell. The size and parameters of the glass are selected so that the rotation of the plane of polarization of the detection beam  $E_s$  at the entrance of the cell relative to the  $z$  axis corresponds to the angle:

$$\xi(t, 0) = -VH_1 l, \quad (23)$$

where  $V$  is the Verde constant of magnetoactive glass,  $l$  is the length of the glass.

To obtain an analytical expression of the photocurrent  $i_\phi$  at the output of the photo recorder after the passage of beam  $E_s$  through the magneto-active glass, gas cell, and polarizer 2 for  $\omega_r \neq 0$ , I shall use the formalism of the Jones method, according to which the electric field of a polarized light wave is represented in the form of a vector:

$$E = \begin{pmatrix} E_z \\ E_y \end{pmatrix}, \quad (24)$$

where  $E_z, E_y$  are scalar components of the electric vector along the  $z$  and  $y$  axes.

The ideal polarizer 2, whose transmission axis is directed along the  $y$  axis, is matched by the matrix:

$$P = \begin{pmatrix} 0 & 0 \\ 0 & 1 \end{pmatrix}, \quad (25)$$

The following matrix corresponds to the magnetoactive glass placed in the transverse magnetic field  $H_1$ :

$$F = \begin{pmatrix} \cos(\xi(t, 0)) & -\sin(\xi(t, 0)) \\ \sin(\xi(t, 0)) & \cos(\xi(t, 0)) \end{pmatrix}. \quad (26)$$

A gas cell is represented by a matrix:

$$\Phi = \begin{pmatrix} \cos(\xi(t, \omega_r)) & \sin(\xi(t, \omega_r)) \\ -\sin(\xi(t, \omega_r)) & \cos(\xi(t, \omega_r)) \end{pmatrix}. \quad (27)$$

The components of the light field vector in front of the DVR are found from the matrix equation:

$$\begin{pmatrix} E_z \\ E_y \end{pmatrix} = \begin{pmatrix} 0 & 0 \\ 0 & 1 \end{pmatrix} \begin{pmatrix} \cos(\xi(t, \omega_r)) & \sin(\xi(t, \omega_r)) \\ -\sin(\xi(t, \omega_r)) & \cos(\xi(t, \omega_r)) \end{pmatrix} \times \\ \times \begin{pmatrix} \cos(\xi(t, 0)) & -\sin(\xi(t, 0)) \\ \sin(\xi(t, 0)) & \cos(\xi(t, 0)) \end{pmatrix} \begin{pmatrix} 1 \\ 0 \end{pmatrix} = \\ = \begin{pmatrix} 0 \\ -\sin[\xi(t, \omega_r) - \xi(t, 0)] \end{pmatrix}. \quad (28)$$

The photo current of the photo recorder  $i_\phi$  is proportional to the radiation power  $I$  falling on its photosensitive area. The intensity of beam  $I$  is equal to the sum of the squares of the amplitudes of individual components:

$$\Delta i_\phi(t, \omega_r) \sim I = E_z^2 + E_y^2 = \sin^2[\xi(t, \omega_r) - \xi(t, 0)]. \quad (29)$$

The normalized photocurrent amplitude  $i\Delta_\phi(t, \omega_r)$  changes from zero at  $\omega_r t = 2\pi k$  to 1.

Fig. 5 shows the time dynamics of the photocurrent  $i\Delta_\phi(t, \omega_r)$  after the low-pass filter. Rectangular pulses are formed in the registered zeros of the signal, which determine the frequency of slow precession of nuclear magnetization  $\omega_r$ :

$$(\omega_r)_i = \frac{2\pi}{\Delta t_i}, \quad (30)$$

where  $\Delta t_i = t_i - t_{i-1}$  is the time interval between adjacent pulses  $i\Delta_\phi(t, \omega_r)$ .

During the observation time  $t$ , pulses corresponding to time intervals  $\Delta t_i$  are received from the counter to the CD input. In each series of  $k$  measurements, the following is determined:

$$\langle \Delta t \rangle = \frac{\sum_{i=1}^k \Delta t_i}{k}, \quad (31)$$

and variance:

$$\sigma^2 = \frac{\sum_{i=1}^k (\Delta t_i - \langle \Delta t \rangle)^2}{k}. \quad (32)$$

Samples (31) are a sequence of random variables. During the measurement time  $t$ , the goniometer makes  $k$  revolutions:

$$k = \frac{t}{\langle \Delta t \rangle}. \quad (33)$$

The pulses of the variable frequency generator (VFG) built into the CD, with a given period of their passage  $\tau$  ( $\tau \ll \Delta t$ ), fill the time interval  $\Delta t$ . The frequency of VFG is chosen in such a way that during the period of the platform turnover  $\Delta t$  the number of pulses is an integer,  $n_{2\pi} = \frac{\Delta t}{\tau} = \frac{2\pi}{\phi_1}$ ,

where  $\phi_1$  is the price of the pulse. During continuous rotation of the nuclear goniometer with a constant angular velocity, periodic self-calibration is carried out on the  $2\pi$  angle standard. The time  $t_\phi$ , the countdown of which begins with the  $(i-1)$ -th pulse formed by the digital LF filter, corresponds to the measured angle and contains  $n_\phi$  clock pulses,  $n_\phi = \frac{t_\phi}{\tau}$ . The result of the angle measurement, expressed in units of clock pulses, is given in the form:

$$\langle \phi \rangle = 2\pi \frac{n_\phi}{n_{2\pi}}. \quad (34)$$

Since only a whole number of pulses is counted, the nuclear goniometer should be considered as a discrete converter with a pulse price  $\phi_1 = \frac{2\pi}{n_{2\pi}}$ , the measurement range is  $360^\circ$ .

The maximum error due to quantization in absolute value does not exceed half the value of the pulse:

$$|q|_{\max} \leq 0.5\phi_1. \quad (35)$$

During the measurement time  $t = k \Delta t > k$  uncorrelated measurements of time intervals  $\tau_i$  take place. To reduce the error, the average value of the time intervals is determined as:

$$\langle \tau \rangle = \frac{1}{k} \sum_{i=1}^k \tau_i, \quad (36)$$

and the variance of error in the mean value is  $\sigma(\langle \tau \rangle)$ . The root mean square error of the mean is defined as the root of the variance. The method of statistical averaging makes it possible to reduce the error by  $\sqrt{k}$  times compared to the error of a single measurement.

The frequencies of magnetization vectors of precessing  $^j\text{Xe}$  isotopes in the inertial frame of reference are written as:

$$\omega_j = \gamma_{j\text{Xe}} B_0 + \omega_r \quad (37)$$

and are informative measurements.

It follows from (37) that the frequency of slow precession of nuclear magnetization  $\omega_r$  is expressed in terms of the precession frequencies of  $^j\text{Xe}$  isotopes:

$$\omega_r = \frac{\gamma_{131}\omega_{129} - \gamma_{129}\omega_{131}}{\omega_{129} - \omega_{131}} = \alpha_{131}\omega_{129} - \alpha_{129}\omega_{131}, \quad (38)$$

where:

$$\alpha_{129} = \frac{|\gamma_{129}|}{|\gamma_{129}| + |\gamma_{131}|} = 0.7713, \quad (39)$$

$$\alpha_{131} = \frac{|\gamma_{131}|}{|\gamma_{129}| + |\gamma_{131}|} = 0.2287. \quad (40)$$

The measurement error of the time intervals  $\Delta t_k$  is related to the fluctuations of the precession frequency  $\omega_r$ , which is a random process with a normal distribution law (11) and depends on the stability of the magnetic field  $B_0$ , the temperature of the cell  $T$ , and the intensity of the pumping radiation  $I_p$ . The relative fluctuations of the time intervals and the frequency of precession are the same:

$$\frac{\delta(\Delta t)}{\langle \Delta t \rangle} = \frac{\delta(\omega_r)}{\langle \omega_r \rangle}, \tag{41}$$

the signal-to-noise ratio is also preserved for them.

Stabilization of the constant external magnetic field  $B_0$  is carried out using feedback on the Helmholtz coils by comparing the reference frequency with the total frequency  $\omega_+$ :

$$\omega_+ = \omega_{129} + \omega_{131} = (\gamma_{129} + \gamma_{131})B_0. \tag{42}$$

The frequency  $\omega_+$  does not depend on the rotation of the sensor and is proportional to the magnetic field  $B_0$ .

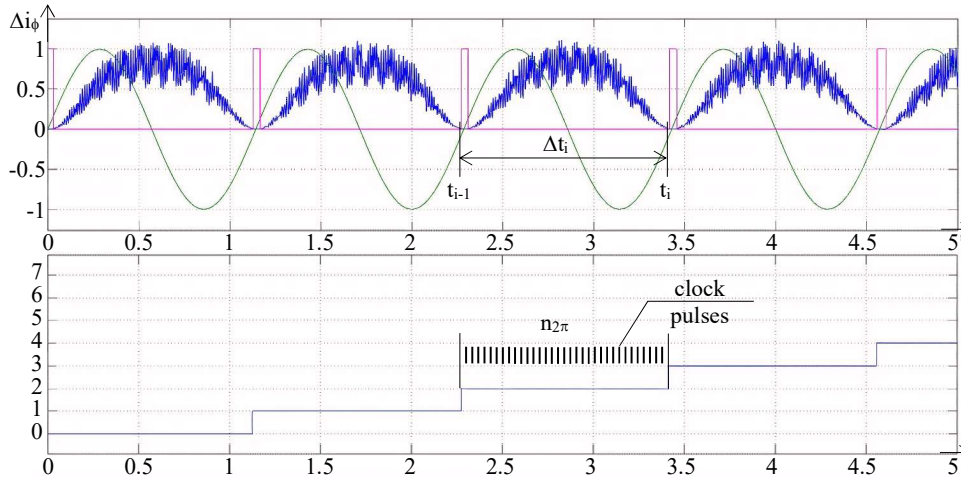


Fig. 5. Time dynamics of the photocurrent  $\Delta i_\phi(t, \omega_r)$  after the low-pass filter

5. 2. 2. Goniometer signal noise

The output signal of the goniometer  $S_{out}$  (22) is narrow-band with a constant amplitude  $A$  ( $A = \text{const}$ ) and a random fluctuation phase  $\delta\phi(t)$  with a uniform distribution. Fluctuations of the nuclear precession phase  $\delta\phi(t)$  are considered to be a stationary Gaussian process. Fig. 6 shows a vector diagram illustrating the change in the phase of the signal under the influence of noise.

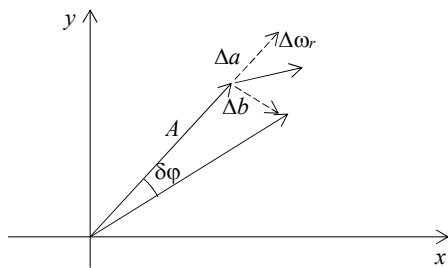


Fig. 6. Vector diagram illustrating the change of precession phase under the influence of noise

Random functions  $\Delta a$  and  $\Delta b$  take zero mean values and equal variances,  $\langle \Delta a \rangle = \langle \Delta b \rangle = 0$ ;  $\langle \Delta a^2 \rangle = \langle \Delta b^2 \rangle = \sigma^2$ . During the averaging time of phase fluctuations, the precession frequencies are equal to zero,  $\langle \Delta\phi(t) \rangle = 0$ , the measurement time is:

$$t = \sum_i \Delta t_i = k \cdot \Delta t, \tag{43}$$

where  $\Delta t$  is the correlation interval.

Dispersion determines the average intensity of signal fluctuations relative to its average value and characterizes noise.

Realizations separated in time by more than the correlation interval are considered uncorrelated. During the measurement of the phase fluctuation of the precession frequency in a series of  $k$  measurements relative to the average value, it takes the form:

$$\Delta\phi(t) = \sum_{i=1}^k \delta\phi_i = \sum_{i=1}^k \frac{\Delta b_i}{A}, \tag{44}$$

where  $\Delta b_i$  is the difference between the final and initial values of  $\Delta\omega_r$  at the time interval  $\Delta t_i$ .

The average value of the square of the phase:

$$\begin{aligned} \langle \delta\phi^2 \rangle &= \\ &= \sum_{i=1}^k \sum_{j=1}^k \frac{\Delta b_i \Delta b_j}{A^2} = \\ &= \frac{1}{A^2} \sum_{i=1}^k \Delta b_i^2 = \\ &= \frac{(\Delta b)^2}{A^2 \Delta t} t = \\ &= \frac{\sigma^2}{A^2 \Delta t} t, \end{aligned} \tag{45}$$

is constantly drifting:

$$\langle \delta\phi^2 \rangle = Dt, \tag{46}$$

where  $D = \frac{\sigma^2}{A^2 \Delta t}$  phase information is lost over time, over  $t = D^{-1}$  the precession phase becomes unpredictable.

The amplitude of the phase fluctuation at the precession frequency due to noise is estimated by:

$$\delta\phi = \sqrt{\langle \delta\phi^2 \rangle} = \frac{1}{(S/N)} \sqrt{\frac{t}{\Delta t}}, \tag{47}$$

where  $(S/N) = \frac{A}{\sigma_{tot}}$  is the signal/noise ratio;

$\sigma_{tot} = \sqrt{\sum_i (\sigma_i)^2}$  is the total effect of noise.

The signal-to-noise ratio determines the error of measuring the angle of rotation of the object:

$$S/N = \frac{\langle S \rangle}{\sigma}. \tag{48}$$

Phase fluctuation can be considered as frequency modulation. At the measurement frequency  $\Delta f \sim 100$  Hz, the observation time  $t \sim 100$  s and the ratio  $(S/N) \sim 10^2$ , the phase shift of the precession frequency due to noise is equal to  $\delta\phi \sim 1$  rad, that is, the measurement of the precession phase of an individual atom during time  $t$  is characterized by an uncertainty of 1 rad.

RMS amplitude of signal noise:

$$\sigma_v = \sqrt{\frac{N_{at}}{\Delta t \cdot t}} = \sqrt{\frac{N_{at}}{\Delta t}} \sqrt{2\Delta f}, \tag{49}$$

where  $\Delta f$  is the frequency band corresponding to the measurement time  $t$ ,  $t = \frac{1}{2\Delta f}$ .

The error of a single measurement of the precession frequency is:

$$\delta\omega_{Rb} = \frac{\sigma_{tot}}{\langle P_{Rb} \rangle S \Delta t} = \frac{1}{\langle P_{Rb} \rangle (S/N) \Delta t}. \quad (50)$$

In the case of multiple measurements during the time  $t \gg \Delta t$  in the case of a normal distribution of the result and averaging over  $k = \frac{t}{\Delta t}$  independent measurements, the error of a single measurement is reduced by  $\sqrt{k}$  times. The angular error accumulated during the measurement time  $t$  is equal to:

$$\delta\varphi = \delta\omega_{Rb} \cdot t = \frac{\sqrt{t}}{\langle P_{Rb} \rangle (S/N) \sqrt{\Delta t}}. \quad (51)$$

Atomic projection noise is statistical, determined by the finite number of atoms and the possible values of the projections of their moments. For white noise, the width of the frequency interval  $\Delta f$  is equivalent to the time interval  $t$  and is  $\Delta f = \frac{1}{2t}$ . Expression for the integral mean square amplitude  $\sigma_{at}$  of such noise in the band  $\Delta f$ :

$$\sigma_{at} = \frac{\sqrt{N}}{t} = \sqrt{\frac{N_{at}}{t \cdot T_2}} = \sqrt{\frac{N_{at}}{T_2}} \cdot \sqrt{2\Delta f}. \quad (52)$$

RMS noise amplitude for Xe isotopes:

$$\sigma_{jXe} = \sqrt{\frac{n_{jXe} V}{t \cdot T_2^{jXe}}}. \quad (53)$$

The error of angle measurement by a goniometer with a differential scheme, caused by projection noises  $^{129}\text{Xe}$  and  $^{131}\text{Xe}$ , is:

$$\delta\varphi_{at} = \sqrt{(\alpha_{131} \delta\varphi_{129Xe})^2 + (\alpha_{129} \delta\varphi_{131Xe})^2}, \quad (54)$$

where, based on (47):

$$\delta\varphi_{jXe} = \frac{\gamma_{jXe}}{\gamma_{Rb}} \cdot \frac{\sqrt{R_{op} + R_{Rb}}}{P_x^{Rb} \sqrt{n_{Rb} V}} \sqrt{t}. \quad (55)$$

Fractional noise that arises due to the discreteness of photons in optics. At the average intensity of photons per unit of time  $\langle N_{ph} \rangle$  the average number of electrons emitted by the photocathode during the observation time  $t$ :

$$\langle N_e \rangle = \eta \langle N_{ph} \rangle t, \quad (56)$$

where  $\eta$  is the average number of electrons emitted by the photocathode when one photon falls on it, usually  $\eta \sim 0.2 \dots 0.3$ . In Gaussian statistics, the root mean square deviation of the number of electrons:

$$\sigma_e = \sqrt{\eta \langle N_{ph} \rangle t}, \quad (57)$$

is equal to their average value for the measurement interval, from this condition it follows that:

$$\langle N_{ph} \rangle = \frac{1}{t\eta}. \quad (58)$$

If one considers that  $N_{ph} = N_{Rb} \frac{t}{T_2}$ , the root mean square amplitude of fractional noise:

$$\delta\varphi_{ph} = \frac{\sqrt{N_{ph}}}{t} = \sqrt{\frac{n_{Rb} V}{\eta t \cdot T_2^{Rb}}}. \quad (59)$$

The total effect of fractional and projection noise is represented by the formula:

$$\sigma_{sum} = \sqrt{\sigma_{ph}^2 + \sigma_{129Xe}^2 + \sigma_{131Xe}^2}. \quad (60)$$

The angular error of the goniometer due to these noises is:

$$\delta\varphi_{sen} = \sqrt{(\alpha_{131} \delta\varphi_{129sen})^2 + (\alpha_{129} \delta\varphi_{131sen})^2}, \quad (61)$$

where:

$$\delta\varphi_{jxen} = \frac{\gamma_{jXe}}{\gamma_{Rb}} \frac{\sigma_{sum}}{P_x^{Rb} S_{jout}} \sqrt{\frac{t}{T_2^{jXe}}}, \quad (62)$$

corresponds to the maximum angular sensitivity.

Fig. 7 shows the angular error of the goniometer (61) depending on the temperature in the cell  $T$  and the laser pumping power  $I_p$ .

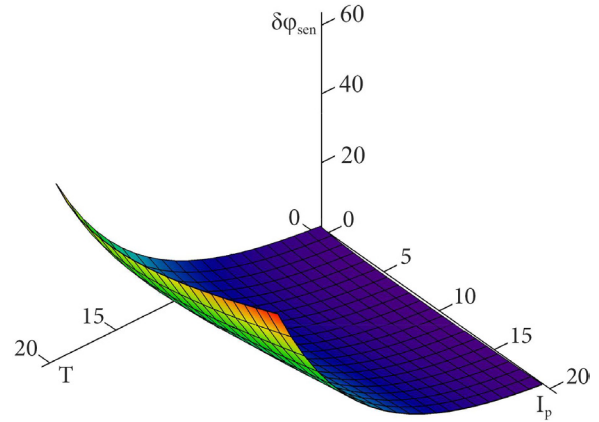


Fig. 7. Angular error of the goniometer  $\delta\varphi_{sen}$  (61)

According to the determined extremum (minimum) of function (61), the optimal values of the working temperature of the gas cell and the optical pumping power are selected. This determines the value of the concentration of  $^{j}\text{Xe}$  isotopes, saturated Rb vapors, and the relaxation time of these components, which increases the sensitivity of the goniometer.

### 5. 2. 3. Root mean square error of the signal based on the permissible values of parameters

The output signal of the goniometer  $S_{out}$  (22) is a function of several independent measured parameters, the stability of which affects the accuracy of determining the angle of rotation of the object  $\phi$ :

$$S_{out} = F(I_p, B_0, T). \quad (63)$$

If the average absolute measurement error of parameter  $x$  is equal to  $\pm \Delta x$ , then the error in the output signal is determined by the expression:

$$\Delta S_{out} = \pm \frac{dF(x)}{dx} \Delta x, \quad (64)$$

And the relative measurement error of the output signal is:

$$\frac{\Delta S_{out}}{S_{out}} = \pm \frac{dF(x)}{dx} \frac{\Delta x}{F(x)} \tag{65}$$

The mean square error  $S_{out}$  is determined from the formula:

$$\sigma_{out} = \sqrt{\left(\frac{\partial F}{\partial I_p}\right)^2 \cdot \sigma_p^2 + \left(\frac{\partial F}{\partial B_0}\right)^2 \cdot \sigma_{B_0}^2 + \left(\frac{\partial F}{\partial T}\right)^2 \cdot \sigma_T^2} \tag{66}$$

where  $\sigma_i$  are the mean square errors of measurements of  $i$ -th quantities.

Fig. 8, 9 show plots of partial derivatives of the signal (22)  $\left(\frac{\partial F}{\partial I_p}\right)_j$ .

In the pump power range (2...10) mW, the values of the partial derivatives  $\left(\frac{\partial F}{\partial I_p}\right)_j$  decrease with the increase in  $I_p$ , at the same time  $\left(\frac{\partial F}{\partial I_p}\right)_{131} > \left(\frac{\partial F}{\partial I_p}\right)_{129}$  by approximately 3 times. Approximate values:

$$\left(\frac{\partial F}{\partial I_p}\right)_{129} \sim 5 \cdot 10^{17}, \quad \left(\frac{\partial F}{\partial I_p}\right)_{131} \sim 1.5 \cdot 10^{18}$$

In the temperature range (100...200) °C, the partial derivatives  $\left(\frac{\partial F}{\partial T}\right)_j$  grow exponentially with increasing  $T$ . At 130 °C approximate values are:

$$\left(\frac{\partial F}{\partial T}\right)_{129} \sim 1.6 \cdot 10^{17},$$

$$\left(\frac{\partial F}{\partial T}\right)_{131} \sim 4.9 \cdot 10^{17}.$$

The accuracy of measuring the angle of rotation of the object is also determined by the accuracy of stabilization of the constant longitudinal magnetic field  $B_0$ . The error of the rotation angle, which is determined by the instability of the magnetic field  $B_0$ , is:

$$\delta\varphi_j = \delta B_0 \omega_j t, \tag{67}$$

where  $\delta B_0$  is the relative error of the constant magnetic field.

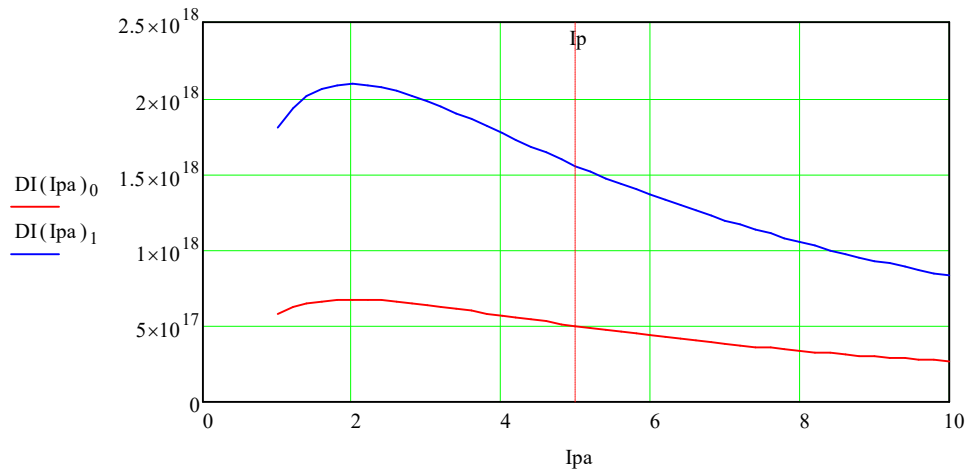


Fig. 8. Plot of dependence of the partial derivative  $\left(\frac{\partial F}{\partial I_p}\right)_j$  on the laser pumping intensity  $I_p$

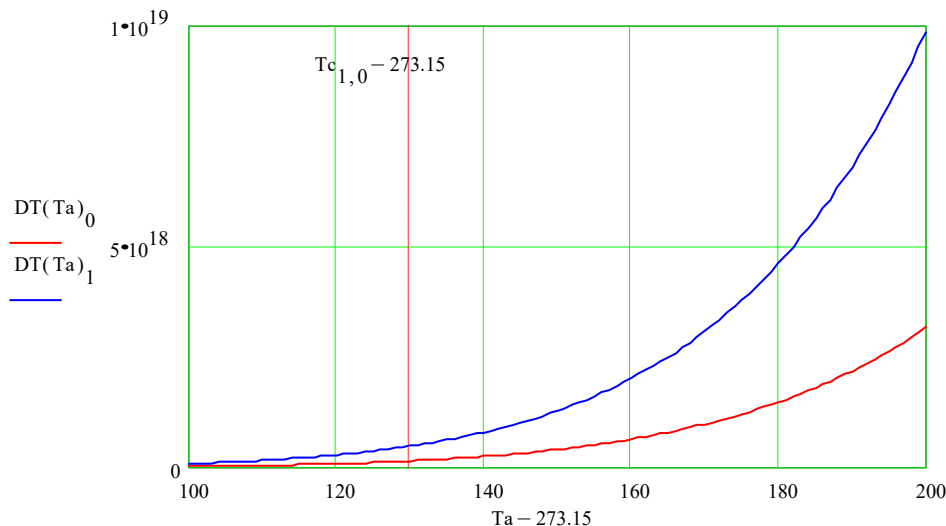


Fig. 9. Plot of dependence of the partial derivative  $\left(\frac{\partial F}{\partial T}\right)_j$  on the temperature in the cell

The errors of the frequency of precession of the  $^j\text{Xe}$  nuclei, calculated from the fluctuations of the measured values of function (63), take the form:

$$\delta\omega_j = \frac{\gamma_{j\text{Xe}}}{\gamma_{\text{Rb}}} \times \sqrt{\left(\frac{\partial F}{\partial I_p}\right)^2 \cdot \left(\frac{\Delta I_p}{I_p}\right)^2 + \left(\frac{\partial F}{\partial B_0}\right)^2 \cdot \left(\frac{\Delta B_0}{B_0}\right)^2 + \left(\frac{\partial F}{\partial T}\right)^2 \cdot \left(\frac{\Delta T}{T}\right)^2} \sqrt{\frac{\Delta f}{t}} \omega_j. \quad (68)$$

Mean square angular error of the goniometer according to the measured parameters (62):

$$\delta\varphi_{\text{tech}} = \sqrt{(\alpha_{131}\delta\varphi_{129})^2 + (\alpha_{129}\delta\varphi_{131})^2}. \quad (69)$$

Total angular error of the goniometer for the considered noises (projection and fractional) and parameters (62):

$$\delta\varphi_{\text{tot}} = \sqrt{(\delta\varphi_{\text{sen}})^2 + (\delta\varphi_{\text{tech}})^2}. \quad (70)$$

The period of passage of clock pulses is selected from the condition:

$$\tau \leq \frac{\delta\varphi_{\text{tot}}}{360 \cdot 3600} \langle \Delta t \rangle, \text{ s.}$$

The main technical factors that determine the angular error are the stability of the temperature in the cell, the stability of the magnetic field, the power and composition of the pumping radiation.

## 6. Discussion of results of investigating the accuracy characteristics of the nuclear goniometer

The following input parameters were used to calculate the full angular error of the goniometer: the volume of the small sensitive element (cell)  $V=8 \text{ cm}^3$ ; according to the determined extremum of the function (61) from Fig. 7, the optimal values of the operating temperature of the gas cell and the optical pumping power were selected: operating temperature  $130 \text{ }^\circ\text{C}$ , laser radiation intensity (pumping and detection)  $I_{p,s} \sim 5 \text{ mW}$ . The concentration of Rb at a temperature of  $130 \text{ }^\circ\text{C}$  according to (3) is  $n_{\text{Rb}}=3.6 \cdot 10^{13} \text{ cm}^{-3}$ ; stabilization of the working temperature is carried out with an accuracy of  $\Delta T=\pm 0.1 \text{ }^\circ\text{C}$ ; relative accuracy of stabilization  $\Delta I_p/I_p=0.05$ .

The maximization of the pumping speed  $R_{op}$  is achieved by maintaining the balance of the concentration of vapors Rb, the intensity of the light beam  $I_p$ , the width of the emission line  $\Delta\nu_p$ , the width of the absorption line  $\Delta\nu_{\text{Rb}}$  according to (2). For numerical calculations, the value  $\Delta\nu_p=0.9 \text{ GHz}$  is used, which is determined by the choice of the radiation source (for example, small lasers of the VCSEL type). The laser emission linewidth  $\Delta\nu_p$  and the Rb absorption linewidth  $\Delta\nu_{\text{Rb}}$  must be matched. If the width of the radiation line is  $\Delta\nu_p \gg \Delta\nu_{\text{Rb}}$ , then a significant number of photons is outside the resonant absorption frequency of Rb atoms, these photons do not contribute to optical pumping, which leads to a loss of light energy, a decrease in absorption and polarization. With a narrow line width  $\Delta\nu_p < \Delta\nu_{\text{Rb}}$ , complete absorption of the laser beam in the cell is possible, in which case there is no signal at the output. The optimal width  $\Delta\nu_p$  for maximum polarization of Rb is a function of

temperature, cell size, and gas mixture component concentrations.

The cell is filled with gases  $^{129}\text{Xe}$ ,  $^{131}\text{Xe}$ ,  $\text{N}_2$  according to (4) with concentrations  $n_{129}=6.5 \cdot 10^{16} \text{ cm}^{-3}$ ,  $n_{131}=2.3 \cdot 10^{17} \text{ cm}^{-3}$ ,  $n_{\text{N}_2}=1.6 \cdot 10^{18} \text{ cm}^{-3}$ , which is higher than the concentration of Rb by (3...4) orders. At  $B_0=10 \text{ } \mu\text{T}$ , the Larmor precession frequency of isotopes  $^{129}\text{Xe}$  and  $^{131}\text{Xe}$  is  $\omega_{129}=119 \text{ Hz}$  and  $\omega_{131}=35.2 \text{ Hz}$ , respectively, the ratio of concentrations is  $n_{129} \approx n_{131} \approx 1 \div 4$ .

The amplitude of the magnetic field created by the currents in the Helmholtz coils,  $B_0=10^{-5} \text{ T}$ , is stabilized with a relative accuracy of  $\Delta B_0/B_0 \approx 1 \cdot 10^{-8}$  (including the shielding of the Earth's magnetic field,  $B_E=5 \cdot 10^{-5} \text{ T}$  and parasitic extraneous magnetic field fluctuations).

The marginal angular error accumulated during the measurement time  $t=1 \text{ s}$  (with complete suppression of technical noises) is, according to (61),  $\delta\varphi_{\text{sen}}=1.0 \text{ arcsec}$ .

The mean quadratic angular error of the goniometer along the channels of Xe isotopes, caused by the errors in the magnetic field and pump parameters, at the sampling time  $\Delta t=10^{-2} \text{ s}$  and  $B_0=10 \text{ } \mu\text{T}$ , according to (69), is  $\delta\varphi_{\text{tech}}=13.6 \text{ arcsec}$ . Therefore, the complete angular error of the goniometer based on noise (projection and fractional) and parameters (62) will be, in accordance with (70),  $13.7 \text{ arcsec}$ .

The biggest contribution to the angle measurement error is from the instability of the pumping power ( $\Delta I_p=\pm 0.05$ ) 85 %; instability of the magnetic field  $B_0$  ( $\Delta B_0/B_0=10^{-8}$ ) contributes 13 %, temperature instability ( $\Delta T=\pm 0.1 \text{ }^\circ\text{C}$ ) – 2 %.

Thus, the model of goniometer errors given in the work makes it possible to estimate the size and structure of the total angle measurement error. The calculation results allow me to state that the error value of the goniometer, calculated according to the model given in this work, is comparable to the error of a classic dynamic goniometer of the medium accuracy class,  $\delta\varphi_{\text{tot}} \geq 10 \text{ arcsec}$  [4, 6].

Therefore, the technical result of using a small-sized sensitive element based on nuclear magnetic resonance is to reduce the energy consumption of the goniometer, to ensure measurements at low speeds of rotation of the object table. The result is also a simplification of the structure of the goniometer and a reduction of its dimensions.

The use of a nuclear goniometer makes it possible to measure angles at low rotation speeds during the manufacture of objects of complex shape, for example, large mirrors.

The limitation of this study is that my estimates of goniometer errors are valid for goniometers with a volume of a small-sized sensitive element  $V=8 \text{ cm}^3$ . Miniaturization of the device by reducing the volume of the sensitive element to  $1 \text{ cm}^3$  or less would require appropriate selection of the laser radiation spectrum width, operating temperature, laser radiation intensity (pumping and detection), and gas concentrations.

A drawback of this study that should be noted is that it is purely theoretical in nature. Experimental verification of the results could be an area of further research. To confirm the correctness of my theoretical statements and calculations, it is advisable to build a test model of a nuclear goniometer and conduct practical verification, which could be the topic of further research. It should be noted that this would require using high-precision equipment for the manufacture of device components, in particular cells, Helmholtz coils, and magnetic field induction stabilization systems.

The considered nuclear goniometer could be used as part of an angle measuring automated system used in optical production for operational control, calibration, and certification of optical products. To improve the angular accuracy of the goniometer, it is necessary to increase the stability of the laser pumping intensity  $I_p$ .

Further research may aim at finding ways to reduce the instability of the laser pumping intensity and improve accuracy of the device.

---

## 7. Conclusions

---

1. As a result of the research, by analyzing the interaction of the gas mixture of  $^{129}\text{Xe}$ ,  $^{131}\text{Xe}$ ,  $\text{N}_2$  isotopes, the pumping radiation and the magnetic field, the dependence of the output signal of the goniometer on parameters of the gas mixture and optical pumping has been established. The nature of this dependence is complex, the output signal of the device is proportional to the transverse polarization  $R_b$ , which is detected by a linearly polarized beam and depends nonlinearly on the partial pressure of components of the gas mixture and the laser pumping power. At the same time, for each specific size of the sensitive element (cell), there are optimal temperatures and power at which the power of the output signal is the greatest. For a cell size of  $8\text{ cm}^3$ , the optimal temperature is  $130\text{ }^\circ\text{C}$ , the optimal radiation intensity  $I_{p,s}\sim 5\text{ mW}$ . As the cell volume decreases, the optimal temperature increases, and the optimal radiation power decreases, provided that the cross-sectional area of the laser beam and the area of the entrance window of the cubic cell are equal. This is due to the fact that as the size of the cell decreases, the density of the photon flux increases, therefore, the required laser power decreases.

2. A method for measuring the angle of rotation has been devised, and, by applying the Jones matrices and the equation for the radiation intensity, the type of output signal of the photodetector was determined. The output signal of the photodetector has a complex shape but is periodic; the zero tracking period of this signal is proportional to the precession frequency of nuclear magnetization. Based

on this period, the measured angle of rotation is judged, and the noise of the device affects the measurement of the length of this period.

By analyzing the noise of the goniometer, it has been determined that the main contribution to the error of the goniometer is from the technical fluctuations caused by the instability of the detuning of the radiation frequency with respect to the central frequency of the atomic transition, which is explained by their higher value compared to other components ( $\delta\phi_{\text{sen}}=1.0\text{ arcsec}$ ,  $\delta\phi_{\text{tech}}=13.6\text{ arcsec}$ ). Natural fluctuations caused by the quantum nature of radiation determine the potential accuracy of the goniometer as they cannot be excluded by applying circuitry solutions. The accumulation of large arrays of measurement information in short periods of time and its statistical processing under a dynamic mode makes it possible to minimize the random component of measurement error in the entire range of angles  $0\dots 360^\circ$ .

---

## Conflicts of interest

---

The author declares that he had no conflicts of interest in relation to the current study, including financial, personal, authorship, or any other, that could affect the study, as well as the results reported in this paper.

---

## Funding

---

The study was conducted without financial support.

---

## Data availability

---

The data will be provided upon reasonable request.

---

## Use of artificial intelligence

---

The author confirms that he did not use artificial intelligence technologies when creating the current work.

---

## References

- Zheng, L., Tang, Q., Ma, X., Zhang, Y. (1996). High-precision static and dynamic angular measurements with a ring laser gyroscope Automated Optical Inspection for Industry, 2899, 50–53. <https://doi.org/10.1117/12.253053>
- Pisani, M., Astrua, M., Santiano, M., Beverini, N., Di Virgilio, A., Maccioni, E. et al. (2018). G-LAS: a ring laser gyroscope for high accuracy angle measurements. *Journal of Physics: Conference Series*, 1065, 032009. <https://doi.org/10.1088/1742-6596/1065/3/032009>
- Wie, Z., Yao, H., Ke, L., Jin, Z., Zi, X. (2022). Calibration and Measurement Method of Laser Gyro Goniometer. *Metrology Science and Technology*, 66 (4), 40–47.
- Cherepanska, I. Yu., Bezvesilna, O. M., Sazonov, A. Yu. (2019). Precise Intelligent Goniometric System. *Visnyk of Vinnytsia Politechnical Institute*, 143 (2), 7–14. <https://doi.org/10.31649/1997-9266-2019-143-2-7-14>
- Zou, W., Huang, Y., Lin, H., Xue, Z. (2024). New Application and Research of Ring Laser Gyroscope in the Field of Angle Metrology. *IEEE Transactions on Instrumentation and Measurement*, 73, 1–12. <https://doi.org/10.1109/tim.2024.3449940>
- Mou, J., Pang, B., Huang, T., Ying, G., Shu, X. (2019). A new method to eliminate the misalignment angle in dynamic goniometer based on fiber optic gyro. *Optik*, 193, 162998. <https://doi.org/10.1016/j.ijleo.2019.162998>
- Pang, B., Ying, G., Xue, F., Huang, T., Che, S., Shu, X., Mou, J. (2019). Uncertainty analysis of dynamic goniometer based on fiber optic gyroscope. *9th International Symposium on Advanced Optical Manufacturing and Testing Technologies: Optical Test, Measurement Technology, and Equipment*, 20, 115. <https://doi.org/10.1117/12.2509290>

8. Ivanov, S. V. (2016). Porivnialnyi analiz efektyvnosti vydiv namotky volokna chutlyvoho elementa volokonno-optychnoho hiroskopa v umovakh zminy temperatury. *Naukovi visti natsionalnoho tekhnichnoho universytetu Ukrainy «Kyivskiy politekhnichnyi instytut»*, 1, 99–106.
9. Ivanov, S. V., Muravov, V. V., Oliinyk, P. B. (2024). Pat. No. 156304 UA. *Honiometr. MPK G01B11/26*; No. u202305588; declared: 21.11.2023; published: 05.06.2024, *Bul. No. 23*.
10. Skinner, J. G., Ranta, K., Whiting, N., Coffey, A. M., Nikolaou, P., Rosen, M. S. et al. (2020). High Xe density, high photon flux, stopped-flow spin-exchange optical pumping: Simulations versus experiments. *Journal of Magnetic Resonance*, 312, 106686. <https://doi.org/10.1016/j.jmr.2020.106686>
11. Cates, G. D., Fitzgerald, R. J., Barton, A. S., Bogorad, P., Gatzke, M., Newbury, N. R., Saam, B. (1992). Rb–<sup>129</sup>Xe spin-exchange rates due to binary and three-body collisions at high Xe pressures. *Physical Review A*, 45 (7), 4631–4639. <https://doi.org/10.1103/physreva.45.4631>
12. Li, R., Quan, W., Fang, J. (2017). Polarization Measurement of Cs Using the Pump Laser Beam. *IEEE Photonics Journal*, 9 (6), 1–8. <https://doi.org/10.1109/jphot.2017.2761779>